AMERICAN ACADEMY OF OPHTHALMOLOGY®

X-Linked Retinoschisis

Deep Phenotyping and Genetic Characterization

Michalis Georgiou, MD, PhD,[1,2,3,] Lucia Finocchio, MD, PhD,[1,4,*] Kaoru Fujinami, MD, PhD,[1,2,5,*] Yu Fujinami-Yokokawa, MPH,[2,5,6] Gianni Virgili, MD,[4,7] Omar A. Mahroo, PhD, FRCOphth,[1,2] Andrew R. Webster, MD(Res), FRCOphth,[1,2] Michel Michaelides, MD(Res), FRCOphth[1,2]*

Purpose: To examine the genetic and clinical features in children and adults with X-linked retinoschisis (XLRS).

Design: Single-center consecutive, retrospective, observational study.

Participants: Adults and children with molecularly confirmed XLRS followed up between 1999 and 2020.

Methods: Analysis of genetic, clinical, and retinal imaging findings, including OCT and fundus autofluorescence (FAF), cross-sectionally and longitudinally, was performed.

Main Outcomes Measures: *RS1*, variants, type of variants and phenotype correlations, age of onset, complications rates and types, fundoscopy findings, OCT metrics, FAF patterns, correlations including between best corrected visual acuity (BCVA) and age, and OCT characteristics.

Results: One hundred thirty-two male patients were identified harboring 66 retinoschisin 1 variants, with 7 being novel. The mean age at onset was 16.5 years (range, 0–58 years). Seventy-one patients (71/75 [94.7%]) were symptomatic at presentation; all had decreased best-corrected visual acuity (BCVA). Funduscopy findings were symmetric in 104 patients (104/108 [96.3%]), with the most common finding being macular schisis (82.4%), whereas peripheral retinoschisis was present in 38.9% and macular atrophy was present in 11.1%. Twenty patients (18.5%) demonstrated complications (vitreous hemorrhage, retinal detachment, or both). Mean BCVA was 0.65 logarithm of the minimum angle of resolution (logMAR; Snellen equivalent, 20/89) in the right eye and 0.64 logMAR (Snellen equivalent, 20/87) in the left eye. Mean BCVA change over a mean interval of 6.7 years was 0.04 and 0.01 logMAR for right and left eyes, respectively. A normal FAF pattern was identified in 16 of 106 eyes (15.1%); 45 eyes (42.5%) showed a spoke-wheel pattern, 13 eyes (12.3%) showed foveal hyperautofluorescence, and 18 eyes (17.0%) showed a central reduction in signal. In total, 14 patients demonstrated evidence of progression on FAF over time. On OCT, foveoschisis was observed in 172 eyes (172/215 [80%]), parafoveal schisis was observed in 171 eyes (171/215 [79.5%]), and foveal atrophy was observed in 44 eyes (44/215 [20.5%]). Cystoid changes were localized to the inner nuclear layer (172/181 eyes [95%]), the outer nuclear layer (97/181 [53.6%]), and the ganglion cell layer (92/181 [50.8%]). Null variants were associated with worse final BCVA and aforementioned complications.

Conclusions: X-linked retinoschisis is highly phenotypically variable, but with relative foveal and BCVA preservation until late adulthood, allowing more accurate prognostication. The slowly (often minimally) progressive disease course may pose a challenge in identification of early end points for therapeutic trials aimed at altering the kinetics of degeneration. *Ophthalmology 2022;129:542-551 © 2021 by the American Academy of Ophthalmology. This is an open access article under the CC BY license (http://creativecommons.org/licenses/by/4.0/).*

Supplemental material available at www.aaojournal.org.

X-linked retinoschisis (XLRS; Mendelian Inheritance in Man identifier, 312700) is the most frequent inherited retinal disease (IRD) presenting in young male patients, accounting for approximately 5% of all childhood-onset IRD, with an estimated prevalence of 1 in 15 000 to 30 000.[1,2] It is caused by pathogenic variants in the retinoschisin 1 (*RS1*) gene (Online Mendelian Inheritance in Man identifier, 300839).[3] Retinoschisin-1 protein is expressed in photoreceptors and bipolar cells and has a role in retinal cell adhesion. Retinoschisin-1 variants disrupt the subunit assembly of the protein and lead to alteration of normal retinal cell adhesion, thus resulting in splitting of the neural layers of the retina.[2]

X-linked retinoschisis typically presents in the first to second decade with variable manifestations, including poor visual acuity, strabismus, anisometropia, and unexplained visual loss, but a smaller number of patients demonstrate the disease in infancy with strabismus, nystagmus, bullous retinoschisis, or a combination thereof.[2] Macular examination can reveal the typical spoke-wheel folds (macular schisis), fine white dots resembling drusen-like deposits, nonspecific retinal pigment epithelial changes, and macular atrophy, with the latter being

© 2021 by the American Academy of Ophthalmology
This is an open access article under the CC BY license (http://creativecommons.org/licenses/by/4.0/). Published by Elsevier Inc.
https://doi.org/10.1016/j.ophtha.2021.11.019
ISSN 0161-6420/21

seen in older individuals.[4,5] During the disease course, secondary complications including vitreous or intraschisis hemorrhage, retinal neovascularization, subretinal exudation, retinal detachment (RD), and traumatic rupture of foveal schisis can occur. Approximately 50% of patients also show peripheral retinal changes, including schisis, metallic sheen, pigmentary disturbance, white spiculations, vitreous veils, and neovascularization.[5,6] Natural history and prognosis are not well established and mostly have been explored in small cohorts, with limited follow-up.

Using OCT, foveoschisis has been reported in 78% to 81% of patients with XLRS, and isolated parafoveal schisis has been reported in a further 10%.[7] Schisis cavities can be found in any retinal layer: the retinal nerve fiber layer (RNFL), ganglion cell layer (GCL), inner nuclear layer (INL), outer plexiform layer (OPL), and outer nuclear layer (ONL).[8,9] Nevertheless, intraretinal cysts are found predominantly in the INL, followed by the OPL and GCL.[10] It is unclear what the implications are of the pattern or location of these cavities. Qualitative changes also are seen in the interdigitation zone (IZ), ellipsoid zone (EZ), external limiting membrane, and photoreceptor outer segments (PROSs).[4] An increased inner retinal foveal thickness and a decreased perifoveal inner retinal thickness have been reported to correlate with worse visual acuity.[7] A spoke-wheel pattern of high- and low-intensity signal represents the characteristic fundus autofluorescence (FAF) findings in XLRS resulting from displacement of luteal pigment.[4] Nevertheless, recently it was identified in only approximately half of patients.[6] Normal FAF findings, low signal in the foveal region, an area of low signal surrounded by a ring of increased signal intensity, or irregular or regular concentric areas of high- and low-intensity FAF can also be observed.[4]

It is imperative to understand the natural progression of the disease and to perform a precise phenotypic characterization when choosing outcome measures to monitor disease progression and outcomes of therapeutic interventions. In this study, we examined the clinical characteristics and the structural and functional outcomes in the largest single-center XLRS cohort reported in the literature, consisting of 132 molecularly confirmed children and adults. We describe their genetic and clinical features, investigate the genotype–phenotype correlations, and establish longitudinal clinical correlations between best-corrected visual acuity (BCVA) and age, OCT characteristics, FAF features, and complications.

Methods

The study adhered to the tenets of the Declaration of Helsinki. Each participant (and a parent of children younger than 18 years) gave written informed consent before genetic testing. Ethical approval was obtained from Moorfields Eye Hospital (London, United Kingdom) for this retrospective single-center observational series.

Participants

Adults and children with XLRS who were examined in the retinal genetics service at a single tertiary center (Moorfields Eye Hospital) were recruited. The XLRS diagnosis was based on clinical findings and family history and was confirmed by detection of a disease-causing *RS1* variant.

RS1 Genetic Analysis

A combination of direct Sanger sequencing and next-generation sequencing, including panels of retinal dystrophy genes, whole exome sequencing, and whole genome sequencing, was used to identify variants in the *RS1* gene. All recruited patients were reassessed for their detected *RS1* variants, as described in the Supplementary Methods (available at www.aaojournal.org).

Ocular Examination and Retinal Imaging

Review of clinical records, including medical and ocular histories, slit-lamp biomicroscopy, and a dilated funduscopic examination, were performed. Age at onset was defined as the patient's age at the first reported symptoms. Best-corrected visual acuity was measured using the Snellen charts and converted into logarithm of the minimum angle of resolution (logMAR) units for statistical analysis. Fundus photography (Optos ultra-widefield camera; Optos UK), infrared reflectance, spectral-domain OCT (Spectralis OCT; Heidelberg Engineering), and short-wavelength (488-nm) FAF were performed longitudinally for most of the patients. Analysis was performed using all available data. Not all methods or tests were always available at the same visit; a different baseline and last follow-up were used to maximize follow-up time for all the studied parameters. The mean age and follow-up time are reported individually for each parameter. The presence of complications, such as vitreous hemorrhage (VH) or RD, were evaluated.

FAF

Spectralis OCT was used to obtain high-resolution FAF images. The data were registered at baseline and at the last follow-up. We identified 4 patterns, and patients were assigned to each group: (1) spoke-wheel pattern, (2) increased central signal, (3) central reduction in signal, and (4) ring of increased signal (Fig 1).

OCT

Spectral-domain OCT was used to obtain high-resolution horizontal line scans of the macula in both eyes of the participants. The data were registered at baseline and at the last follow-up. The presence of foveoschisis, parafoveal schisis, and foveal atrophy was evaluated. Schisis localization using vertical and horizontal central macular OCT images was analyzed by evaluating the RNFL, GCL, INL, OPL, inner plexiform layer (IPL), and ONL. Central macular thickness was calculated automatically using a circular Early Treatment Diabetic Retinopathy Study-type grid positioned on the center of the fovea (central circle of approximately 1-mm diameter) after the scans were reviewed and corrected manually if needed. Defects in the outer retinal photoreceptor microstructures were evaluated, including the IZ and EZ in an area 1 mm from the foveal center, also using vertical and horizontal central OCT images. An IZ defect was defined as an irregularity or a definite defect of the line. Disruptions in the EZ were defined as signal interruptions at the level of the EZ line. Foveal atrophy was defined as total absence of the IZ or EZ bands. The PROS thickness was calculated by manual measurement of the distance between the EZ and the anterior surface of the retinal pigment epithelium, as described previously.[11] The presence of specific OCT findings, including schisis and defects, was determined by consensus between 2 observers (L.F. and M.G.). Any discrepancies between the observers were resolved through discussion with the principal investigator (M.M.) until consensus was reached.

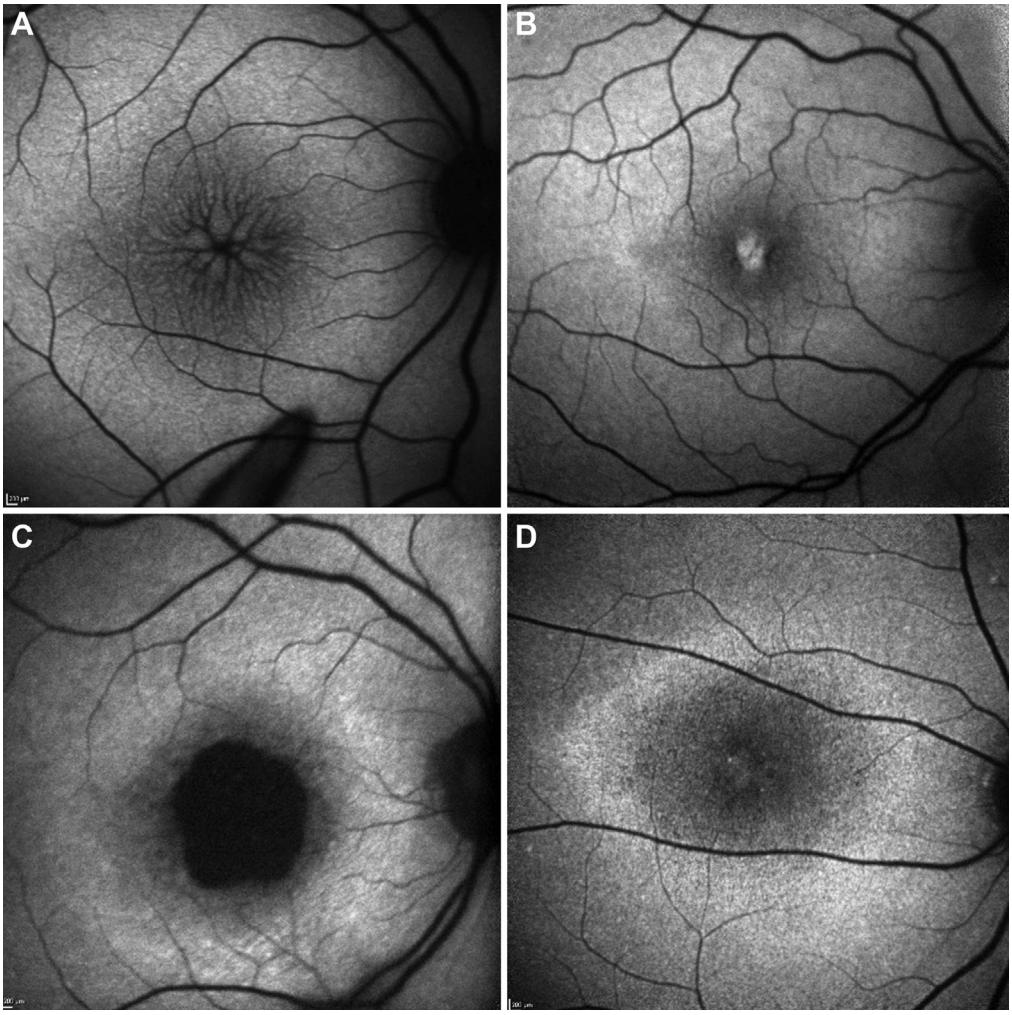

Figure 1. Fundus autofluorescence images showing patterns in X-linked retinoschisis. Four main patterns were identified: (**A**) spoke-wheel, (**B**) increased central signal, (**C**) central reduction in signal, and (**D**) ring of increased signal.

Statistical Analysis

Statistical analysis was carried out using SPSS Statistics for Windows version 22.0 (IBM Corp). Significance for all statistical tests was set at $P < 0.05$. The Shapiro–Wilk test was used to test for normality for all variables.

Results

Demographic Data

We ascertained 132 male patients from 126 families who were followed up between 1999 and 2020. Clinical data and BCVA were available from 1 or more visit for 127 patients. The mean ± standard deviation (SD) age of the group was 25.4 ± 16.7 years (range, 2.3–70.8 years). The baseline age and the follow-up time are indicated below for each assessment.

RS1 Genetic Analysis

All recruited patients harbored pathogenic or likely pathogenic variants in *RS1*. In total, 66 variants were identified. Table 1 presents the 12 most prevalent variants, and Figure 2 presents the localization of the identified variants in the gene domains. The 5 most prevalent variants account for 30.2% of affected families. Seven variants are novel (Table 1). One variant (c.52+5G→C) was identified in cis with the variant c.35T→A in 3 patients from 3 different pedigrees and, based on in silico analysis, may not contribute to disease. Table S1 (available at www.aaojournal.org) presents all sequence variants based on their Human Genome Variation Society nomenclature and their predicted effect. Missense variants were the most common type of alteration (n = 48 [72.7%]). Pathogenicity assessment based on the American College of Medical Genetics and Genomics guidelines, allele frequency, coverage, general and functional prediction scores, and conservation scores of all detected variants are presented in Tables S2, S3, S4, S5, and S6 (available at www.aaojournal.org). Figure S1 (available at www.aaojournal.org) presents evolutionary conservation for detected missense variants.

Disease Onset

Age at onset was recorded in years for 61 patients. The mean ± SD age of onset was 16.5 ± 15.4 years (range, 0–58 years; median, 11

Table 1. Frequent and Novel Variants

Variant (Human Genome Variation Society)*		No.		%	
Complementary DNA	*Protein*	*Patients*	*Pedigrees*	*Patients*	*Pedigrees*
Frequent variants					
c.304C→T	p.(Arg102Trp)	10	10	7.6	7.9
c.574C→T	p.(Pro192Ser)	8	8	6.1	6.3
c.214G→A	p.(Glu72Lys)	8	7	6.1	5.6
c.598C→T	p.(Arg200Cys)	7	7	5.3	5.6
c.35T→A†	p.(Leu12His)	6	6	4.5	4.8
c.421C→T	p.(Arg141Cys)	5	5	3.8	4.0
c.(?_1-1)_(52+1_53-1)del	p.(=)	4	4	3.0	3.2
c.305G→A	p.(Arg102Gln)	8	4	6.1	3.2
c.579dup	p.(Ile194Hisfs*70)	4	4	3.0	3.2
c.589C→T	p.(Arg197Cys)	3	3	2.3	2.4
c.637C→T	p.(Arg213Trp)	3	3	2.3	2.4
c.78G→C	p.(Glu26Asp)	3	3	2.3	2.4
Novel variants					
c.20del	p.Gly7Alafs*119	1	1	0.8	0.8
c.185-1G→A	p.(=)	1	1	0.8	0.8
c.336_337delinsTT	p.Trp112_Leu113delinsCysPhe	1	1	0.8	0.8
c.378del	p.Leu127*	2	2	1.5	1.6
c.435dup	p.Ile146AsnfsTer15	1	1	0.8	0.8
c.515del	p.Asn172Thrfs*65	1	1	0.8	0.8
c.574_580delinsACCCCCCT	p.Pro192Thrfs*72	1	1	0.8	0.8

*Sequence variant nomenclature was obtained according to the guidelines of the Human Genome Variation Society by using Mutalyzer (https://mutalyzer.nl/).
†In 3 patients from 3 different families, the variant c.35T→A was in cis with the variant c.52+5G→C.

years). One patient (1.3%) showed symptoms shortly after birth. Half of the patients were symptomatic before the age of 11 years. Age at baseline examination is detailed in the visual acuity section. Table 2 summarizes the age of onset and all clinical findings. Figure 3A presents the age at onset by age group for the cohort.

Signs and Symptoms

Signs and symptoms were available for 75 patients. Seventy-one patients (94.7%) were symptomatic at presentation. Four patients were asymptomatic at first evaluation and were referred because of a family history of XLRS. A universal finding was reported decreased visual acuity (100%). The clinical presentation varied (Table 2), but symptoms included nyctalopia (n = 6 [8.5%]), strabismus (n = 6 [8.5%]), VH (n = 3 [4.3%], bilateral in 1 case), RD (n = 2 [2.7%]), and nystagmus (n = 1 [1.4%]). No patient demonstrated photophobia or reduced color vision.

Funduscopy findings were documented for 108 patients. Four showed normal fundi. Findings were bilateral in 104 patients (96.3%). The most common finding was macular schisis (89 patients [82.4%]), whereas peripheral retinoschisis was present in 42 patients (38.9%). Atrophic macular thinning was present in 12 patients (11.1%). Only 1 patient showed signs of macular atrophy and schisis. The mean age of patients with macular atrophy was 46.5 years (range, 19–66 years). In contrast, patients with foveal schisis were younger (mean, 22.1 years; range, 3–56 years). Twenty patients (18.5%) demonstrated complications at initial presentation or over follow-up: 8 patients had VH (7.2%), 6 patients had VH and RD (5.6%), and 8 patients had RD without VH (7.2%).

Visual Acuity

Best-corrected visual acuity was assessed cross-sectionally and longitudinally. One hundred twenty-seven patients had BCVA available from 1 or more visits. None had any other vision-limiting disease. Mean ± SD age at baseline was 25.4 ± 16.7 years (range, 2.3–70.8 years). Mean ± SD BCVA was 0.65 ± 0.43 logMAR (range, −0.1 to 3.0 logMAR; Snellen equivalent, 20/89) for the right eye and 0.64 ± 0.44 logMAR (range, 0.0–3.0 logMAR; Snellen equivalent, 20/87) for the left eye at baseline. Baseline BCVA was highly variable among patients, but no significant interocular difference was found ($z = 0.27$, $P = 0.79$, Wilcoxon signed-rank test). A moderate statistically significant correlation was found between mean BCVA for right and left eyes and the baseline age ($r = 0.39$, $P < 0.01$, Spearman's correlation coefficient). Figure 3B presents the mean BCVA against age for the cohort. The moderate correlation may reflect the early severe decrease in BCVA and the further slow decline with age.

One hundred thirteen patients had available longitudinal BCVA data. Mean ± SD follow-up was 6.7 ± 5.2 years (range, 0.2–19.6 years). The mean ± SD BCVA was 0.69 ± 0.56 logMAR (range, −0.10 to 3.0 logMAR; Snellen equivalent, 20/98) and 0.65 ± 0.48 logMAR (range, 0.0–3.0 logMAR; Snellen equivalent, 20/89) for the right and left eyes, respectively, at last follow-up. The mean change over follow-up was 0.04 and 0.01 logMAR for right and left eyes, respectively, without significant interocular difference ($P = 0.38$, $z = 0.88$, Wilcoxon signed-rank test). No significant correlation was found between mean rate of BCVA change for right and left eyes and the baseline age ($r = 0.15$, $P = 0.12$, Spearman's correlation coefficient).

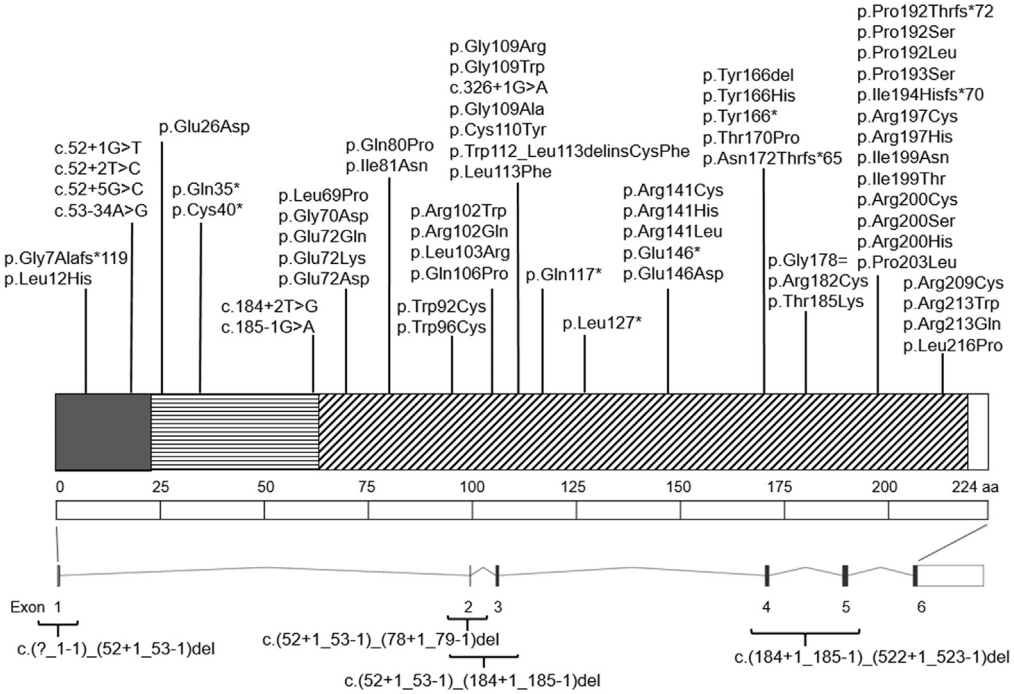

Figure 2. Graphical representation of retinoschisin 1 (*RS1*). *RS1* consists of a signal peptide (amino acids [AA] 1−23, marked with gray), an *RS1* domain (AA 23−62, marked with horizontal lines), and a discoidin domain (AA 63−219, marked with diagonal lines). The identified variants in the current cohort are shown.

FAF

Fundus autofluorescence findings were available for 108 patients for cross-sectional assessment (mean ± SD age, 27.7 ± 16.1 years). Ten patients who had low-quality imaging in 1 eye and 2 patients who had low-quality imaging for both eyes were excluded from analysis. In the remaining 96 patients, FAF pattern was similar bilaterally. For cross-sectional assessment, the right eye was included from each patient (106 eyes from 106 patients).

Normal FAF findings were seen in 16 of 106 eyes (15.1%); 45 eyes (42.5%) showed a spoke-wheel pattern and 13 eyes (12.3%) showed foveal hyperautofluorescence (increased central signal pattern), whereas 18 eyes (17.0%) showed a central reduction in signal. Central hypoautofluorescence surrounded by hyperautofluorescent borders (ring of increased signal) was found in 14 eyes (13.2%); it was isolated in 7 eyes (6.6%), whereas it was associated with spoke-wheel pattern in 3 eyes (2.8%) and with central reduction in signal in 4 eyes (3.8%). The FAF findings at baseline are summarized in Table S7 (available at www.aaojournal.org).

Transition between patterns of FAF was highly variable, with no definite sequence. Progression from normal FAF findings to an increased central signal was observed in 2 eyes after a mean follow-up of 3 years, to a central reduction in signal in 1 eye after 11 years, and to a ring of increased signal in 2 eyes after a mean follow-up of 3.5 ± 0.7 years. A progression from a spoke-wheel pattern to a central reduction in signal was detected in 5 eyes after 6 ± 4.8 years, to an increased central signal in 1 eye after 6 years, to a ring of increased signal in 1 eye after 10 years, and to normal FAF findings in 3 eyes after a mean of 3.3 ± 3.2 years. Progression from an increased central signal to normal findings was observed in 1 eye after 3 years and to a spoke-wheel pattern in 1 eye after 5 years.

OCT

Spectral-domain OCT data were available for 215 eyes of 115 patients at baseline (mean ± SD age, 27.7 ± 17.4 years). Foveoschisis was observed in 172 of 215 eyes (80%), parafoveal schisis was observed in 171 of 215 eyes (79.5%), and foveal atrophy was observed in 44 of 215 eyes (20.5%). The localization of the cavities was mapped for 181 eyes at baseline, localized mainly in the INL (172/181 eyes [95%]) and then in the ONL (97 eyes [53.6%]) and GCL (92 eyes [50.8%]). Cavities were observed in the OPL in 41 eyes (22.7%) and in the IPL in only 1 eye (0.6%). The RNFL was involved in 2 eyes (1.1%). The mean central macular thickness was 378.15 ± 162.13 μm (range, 46−1099 μm).

Qualitative analysis of photoreceptor structure at baseline revealed that the IZ was the most frequently affected area and was found to be disrupted in 139 of 220 eyes (63.2%). Ellipsoid zone analysis was possible in 218 eyes; it was disrupted in 133 eyes (61%). Mean PROS length was 36.9 ± 7.3 μm (range, 15−56 μm). Previously reported mean PROS length for healthy individuals is 47 ± 4 μm (range, 37−54 μm).[10] All OCT findings at baseline are summarized in Table S8 (available at www.aaojournal.org).

Follow-up OCT imaging was available for 187 eyes of 115 patients (mean ± SD age, 30.5 ± 17.3 years). Foveoschisis was observed in 140 of 187 eyes (74.9%), parafoveal schisis was observed in 129 eyes (68.9%), and foveal atrophy was observed in 41 eyes (21.9%). Data on cavities were available for 175 eyes, localized mainly in the INL (164/175 [93.7%]) and then in the ONL (96 eyes [54.9%]) and GCL (85 eyes [48.6%]). Cavities were observed in the OPL in 34 eyes (19.4%). The mean central macular thickness was 348.87 ± 164.15 μm (range, 28−1130 μm). No cavities were detected in the IPL and RNFL.

Table 2. Clinical Findings

Parameter	Data
Age at disease onset (n = 61), yrs	
Mean ± SD	16.5 ± 15.4
Range	0-58
Median	11
Common symptoms and findings at presentation (n = 75), no. (%)	
Reduced BCVA	75 (100)
Nyctalopia	6 (8.5)
Strabismus	6 (8.5)
Vitreous hemorrhage	3 (4.3)
Retinal detachment	2 (2.7)
Nystagmus	1 (1.4)
Funduscopy findings (n = 108), no. (%)	
Bilateral findings	104 (96.3)
Unilateral findings	4 (3.7)
Macular schisis	89 (82.4)
Peripheral schisis	42 (38.9)
Macular atrophy	12 (11.1)
Normal fundus	4 (3.7)

BCVA = best-corrected visual acuity; SD = standard deviation.

Qualitative analysis was performed at the last follow-up, with again the most frequently affected structure being the IZ, with IZ disruption in 119 of 183 eyes (65%). Ellipsoid zone analysis was possible in 184 eyes; it was disrupted in 118 eyes (64.1%). Mean PROS length was 36.38 ± 6.89 μm (range, 22–53 μm) and was similar to baseline (paired *t* test).

Genotype–Phenotype Correlations

The mean ± SD age at onset for patients with null and missense variants was 18.3 ± 15.6 years (range, 3–58 years) and 16.1 ± 15.2 years (range, 0–55 years), respectively, and it was similar between the 2 groups ($P = 0.44$, $z = 0.78$, Mann–Whitney *U* test). The BCVA at last follow-up was worse for patients with null variants (mean ± SD, 0.80 ± 0.49 logMAR; range, 0–2.1 logMAR) compared with patients with missense variants (mean ± SD, 0.63 ± 0.41 logMAR; range, 0–2.2 logMAR); however, the difference was not statistically significant ($P = 0.07$, $z = 1.81$, Mann–Whitney *U* test). From the 22 patients who demonstrated complications (RD, VH, or both), 7 harbored null variants, and 15 harbored missense variants. The frequency of complications is similar among the 2 groups ($P = 0.09$; chi-square, 2.83).

Discussion

The current study described the genetic, clinical, and imaging characteristics of 132 male patients from 126 families with molecularly confirmed XLRS, both cross-sectionally and longitudinally. It represents the largest cohort to date to undergo detailed analysis, including multimodal imaging and genotype–phenotype investigation. Our results provide insights into the retinal phenotype and natural history over a wide range of ages.

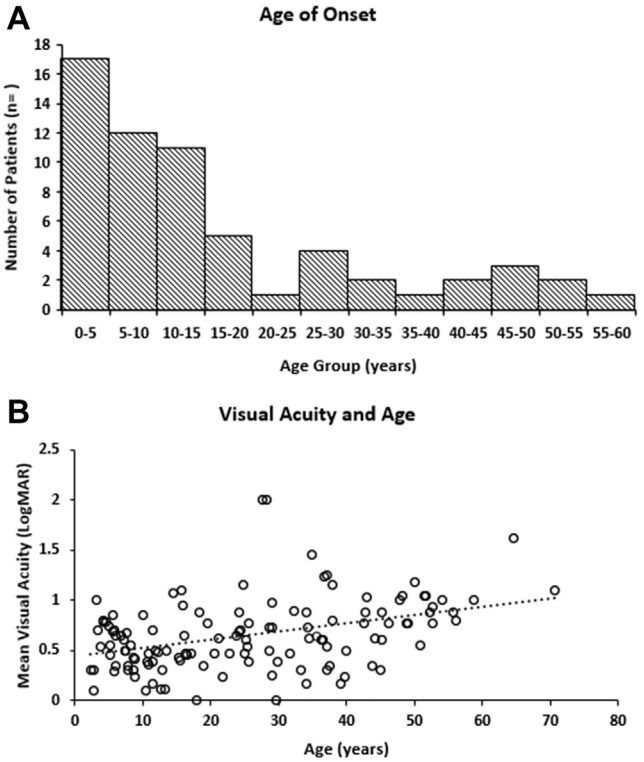

Figure 3. Graphs showing age at onset and visual acuity. **A**, Bar graph showing number of patients by age group for the age of onset, with the vast majority having onset in childhood. **B**, Scatterplot showing the mean best-corrected visual acuity at baseline against age for 127 patients, showing a positive statistically significant correlation. logMAR = logarithm of the minimum angle of resolution.

Genotypic and Phenotypic Variability

More than 200 disease-associated variants in *RS1* are known, with most occurring as nonsynonymous changes in the major protein unit (discoidin domain; Fig 2). In our study, 66 variants were identified, of which 7 were novel. Missense variants were the most common (72.7%), in agreement with previous reports.[12] Phenotypic variability is documented in the literature, with a variety of factors thought to contribute, including the underlying variant and age.[13–17] Other studies report intrafamilial variability and lack of correlation between the type of variant and disease severity or progression.[12,18–20] The most established correlation between genotype and phenotype has been described for electroretinography findings, where patients with null variants showed consistently more severe electroretinography findings.[6,13] The patients in our cohort showed profound phenotypic variability. Age at onset, BCVA at last follow-up, and frequency of complications were not statistically significantly different in this cohort among patients with null and missense variants; however, it should be noted that the BCVA and frequency of complications showed an association with the group with null variants ($P = 0.07$ and $P = 0.09$, respectively) and that final BCVA was on average 0.17 logMAR higher (worse BCVA) in the null variant group.

The clinical characteristics of this cohort are broadly in keeping with those in published reports. The most common retinal finding was macular schisis (n = 89/108 [82.4%]), whereas peripheral retinoschisis was present in more than one third of patients (n = 42/108 [38.9%]). Previous reports identified macular schisis from 68% to 76% of patients, peripheral retinoschisis in 43% to 60% of patients, and macular atrophy in 8% to 10% of patients.[5,16,21] Macular atrophy was present in 12 patients (11.1%), and only 1 patient showed simultaneous findings of macular atrophy and schisis. Some studies have reported macular atrophy in patients in their fourth decade of life and clinical descriptions of macular schisis flattening with age without a clear mechanism for these changes.[14,22] In our study, we found the mean age of patients with macular atrophy was 46.5 years (range, 19−66 years). In contrast, patients with foveal schisis were younger (mean, 22.1 years; range, 3−56 years).

Twenty-two patients (19.8%) demonstrated complications such as VH, RD, or both. The frequency of complications varies considerably in the literature, with a frequency between 3% and 21% for VH and between 5% and 40% for RD.[5,21,23,24] Recently, we reported increased incidence of VH and RD in patients with peripheral schisis.[21] We can hypothesize that the natural history of XLRS often begins with a normal fundus in younger patients; then, retinoschisis develops, with, finally, macular atrophy slowly developing at an older age, which may be complicated further by VH, RD, or both, albeit with a significant age overlap in these aforementioned stages of disease progression.

Best-corrected visual acuity varies widely, with previous studies reporting a mean BCVA of 0.49 to 0.6 logMAR.[5,10,25] Mean BCVA in this study was 0.65 and 0.64 logMAR for the right and left eyes, respectively. Mean change over time was 0.04 and 0.01 logMAR for right and left eyes, respectively (mean follow-up, 6.7 years), without significant interocular difference. These data indicate an overall relative stability, with very slow modest progression over time, in agreement with previous reports.[16,26,27] A moderate statistically significant correlation was found between mean BCVA for right and left eyes and baseline age. The moderate correlation may reflect the early severe decrease in BCVA and further slow decline with age.

Structural Changes and Disease Natural History

Fundus autofluorescence findings were highly variable, including normal FAF findings, spoke-wheel pattern, foveal hyperautofluorescence, and central reduction in signal. Hyperautofluorescent foveal borders (ring of increased signal) was observed in isolation or with central hypoautofluorescence, spoke-wheel, or central signal reduction. Variability in FAF results has been reported.[6,10] Spoke-wheel pattern, although characteristic in XLRS, was identified only in 42.5% of patients (45/106), with a recent report stating 54% (51/94 eyes).[10] We can speculate that progression (albeit not in all patients) occurs from an increased central signal to a spoke-wheel pattern and, finally, to a central reduction in signal.

In keeping with the literature, foveoschisis was seen in 80% of eyes (172/215), parafoveal schisis was seen in 79.5% of eyes (171/215), and foveal atrophy was seen in 20.5% of eyes (44/215).[10,12] Foveal cavities occurred mostly in the INL (95%), OPL (22.7%), and ONL (53.6%) and then the GCL (50.8%).[7,10,28,29] Our findings parallel, especially for INL, those reported by Andreoli and Lim,[7] who found that schisis affected the INL and OPL in 85% and 61% of cases, respectively, and those reported by Orès et al,[10] who identified schisis changes mainly in the INL (88%) and OPL (64%), followed by RNFL, GCL (46%), and ONL (22%). In almost half of eyes, cavities were also found in the GCL in previous reports.[25,29] None were detected in the IPL or RNFL in the last follow-up and in only 3 eyes at baseline (1.7%). These data would be in keeping with the *RS1* protein being distributed widely in the retinal layers. We provide further data to support that the most frequent qualitative defect in outer photoreceptor structure is disrupted IZ, identified in 63.2% of eyes at baseline and in 65% at last follow-up.[10] Ellipsoid zone disruption was observed in 61% at baseline and in 64% at last follow-up. The combined data to date support the hypothesis that the IZ defect may reflect the initial changes in photoreceptors and that anatomic change over time is relatively limited.[25,30]

End Points for Clinical Trials

OCT measurements were the most widely available metric in the cohort, independent of disease state, and, in agreement with a recent report, can provide metrics for clinical trials.[31] OCT measurements have been used as reliable end points in many IRD studies and trials.[32] OCT also can be used for the identification of early disease changes in retinal layers before the development of overt atrophy; however, the slow disease progression identified in our study may pose a challenge in quantification of changes in OCT that exceed the test−retest repeatability within the time frame of a trial. Reliability and repeatability assessment studies with standardized protocols should evaluate the OCT metrics further before use in trials. The FAF metrics, such as area of atrophy, were also previously proven to have good repeatability in IRDs[33]; however, atrophy is evident only in a subset of patients with XLRS and only in advanced disease, thereby limiting the usefulness of this method in trials. Functional assessments beyond BCVA, such as microperimetry testing, as well as more advanced imaging techniques, such as adaptive optics imaging,[34] warrant further exploration in XLRS.

Future Directions

X-linked retinoschisis is an attractive target for gene therapy because of its monogenic nature and promising preclinical studies.[35] The *RS1*-knockout mouse showed rapid structural and functional treatment benefits after intravitreal *RS1* gene replacement.[36,37] Two phase I/II intravitreal gene therapy trials (ClinicalTrials.gov identifiers, NCT02416622 [sponsored by Applied Genetics Technology Corp.] and NCT02317887 [sponsored by the National Eye Institute]) have been conducted: the former was halted because of marked ocular inflammation, whereas the latter added

additional agents to the standard oral steroids used in subretinal gene supplementation trials to address the uveitis adverse events; further efficacy data are awaited.[38]

Study Limitations

The main limitations of our study are the retrospective design, the lack of a control group, and the variable follow-up duration. An additional limitation is the lack of visual field data. Despite these limitations, this study provides a comprehensive analysis of the genetic, structural, and clinical characteristics of the largest XLRS cohort reported in the literature, with long-term follow-up, helping to elucidate disease natural history.

Conclusion

In conclusion, XLRS has a wide spectrum of clinical characteristics; hence, molecular diagnosis is crucial for its early diagnosis and genetic counseling, as well as for potential participation in clinical trials. X-linked retinoschisis has a wide window of therapeutic opportunity, with most patients having relative preservation of foveal structure (and function) until the fourth decade of life; however, the disease has an early onset and often significantly reduced BCVA early in the disease course. The slow disease progression identified in our study may pose a challenge in the identification of early end points for interventions aiming to slow or halt degeneration.

Acknowledgments

The authors thank Xiao Liu, MD, National Institute of Sensory Organs, National Hospital Organization Tokyo Medical Center, Tokyo, Japan, and Lizhu Yang, MD, PhD, Department of Ophthalmology, Keio University School of Medicine, Tokyo, Japan, for their contribution to the in silico genetic analysis and figure creation.

Footnotes and Disclosures

Originally received: September 16, 2021.
Final revision: November 4, 2021.
Accepted: November 9, 2021.
Available online: November 23, 2021. Manuscript no. D-21-01865.

[1] Moorfields Eye Hospital, London, United Kingdom.

[2] UCL Institute of Ophthalmology, University College London, London, United Kingdom.

[3] Jones Eye Institute, University of Arkansas for Medical Sciences, Little Rock, Arkansas.

[4] Department of Neuroscience, Psychology, Drug Research and Child Health, Ophthalmology, University of Florence-Careggi, Florence, Italy.

[5] Laboratory of Visual Physiology, Division of Vision Research, National Institute of Sensory Organs, National Hospital Organization Tokyo Medical Center, Tokyo, Japan.

[6] Department of Health Policy and Management, School of Medicine, Keio University, Tokyo, Japan.

[7] Centre for Public Health, Queen's University Belfast, Belfast, United Kingdom.

*These authors contributed equally as first authors.

Disclosure(s):

All authors have completed and submitted the ICMJE disclosures form.

The author(s) have made the following disclosure(s):

M.G.: Consultant − MeiraGTx; Lecturer − Novartis

K.F.: Consultant − Astellas Pharma, Kubota Pharmaceutical Holdings and Acucela, Janssen Pharma, Novartis Pharma, NightstaRx

M.M.: Consultant − MeiraGTx

Supported by the National Institute for Health Research Biomedical Research Centre at Moorfields Eye Hospital NHS Foundation Trust and UCL Institute of Ophthalmology, London, United Kingdom; Onassis Foundation; Leventis Foundation; The Wellcome Trust (grant nos.: 099173/Z/12/Z and 206619/Z/17/Z); Moorfields Eye Charity, London, United Kingdom; Retina UK; the Foundation Fighting Blindness; the Ministry of Education, Culture, Sports, Science and Technology, Japan (grant nos.: 16H06269 and 16KK01930002 [K.F.]); the National Hospital Organization Network Research Fund (grant no.: H30-NHO-Sensory Organs-03 [K.F.]); the Japan Agency for Medical Research and Development (grant no.: 18992608 [K.F.]); the Ministry of Health, Labour and Welfare (grant no.: 18ek0109355h0001 [K.F.]); the Foundation Fighting Blindness Alan Laties Career Development Program (grant no.: CF-CL-0416-0696-UCL [K.F.]); the Ministry of Health Labour and Welfare (Health Labour Sciences Research Grant no.: 201711107° [K.F.]); the Great Britain Sasakawa Foundation Butterfield Awards (K.F.); and the Italian Ministry of Health and Fondazione Roma under the Aging Network of Italian Research Hospitals (G.V.).

HUMAN SUBJECTS: Human subjects were included in this study. Ethical approval was obtained from Moorfields Eye Hospital for this retrospective single-center observational series.

All research adhered to the tenets of the Declaration of Helsinki. Each subject (and a parent of children <18 years of age) gave written informed consent before genetic testing.

No animal subjects were included in this study.

Author Contributions:

Conception and design: Georgiou, Virgili, Mahroo, Webster, Michaelides

Analysis and interpretation: Georgiou, Finocchio, Fujinami, Fujinami-Yokokawa

Data collection: Georgiou, Finocchio, Fujinami, Fujinami-Yokokawa, Webster, Michaelides

Obtained funding: N/A

Overall responsibility: Georgiou, Finocchio, Fujinami, Virgili, Mahroo, Webster, Michaelides

Abbreviations and Acronyms:
BCVA = best-corrected visual acuity; **EZ** = ellipsoid zone; **FAF** = fundus autofluorescence; **GCL** = ganglion cell layer; **INL** = inner nuclear layer; **IPL** = inner plexiform layer; **IRD** = inherited retinal disease; **IZ** = interdigitation zone; **logMAR** = logarithm of the minimum angle of resolution; **OPL** = outer plexiform layer; **ONL** = outer nuclear layer; **PROS** = photoreceptor outer segment; **RD** = retinal detachment; **RNFL** = retinal nerve fiber layer; ***RS1*** = retinoschisin 1; **VH** = vitreous hemorrhage; **XLRS** = X-linked retinoschisis.

Keywords:
Fundus phenotype, Gene therapy, *RS1*, X-linked retinoschisis, XLRS.

Correspondence:
Michel Michaelides, MD(Res), FRCOphth, UCL Institute of Ophthalmology, University College London, 11-43 Bath Street, London EC1V 9EL, United Kingdom. E-mail: michel.michaelides@ucl.ac.uk.

References

1. Molday RS, Kellner U, Weber BH. X-linked juvenile retinoschisis: clinical diagnosis, genetic analysis, and molecular mechanisms. *Prog Retin Eye Res*. 2012;31(3):195–212.
2. Rahman N, Georgiou M, Khan KN, Michaelides M. Macular dystrophies: clinical and imaging features, molecular genetics and therapeutic options. *Br J Ophthalmol*. 2020;104(4):451–460.
3. Sauer CG, Gehrig A, Warneke-Wittstock R, et al. Positional cloning of the gene associated with X-linked juvenile retinoschisis. *Nat Genet*. 1997;17(2):164–170.
4. De Silva SR, Arno G, Robson AG, et al. The X-linked retinopathies: physiological insights, pathogenic mechanisms, phenotypic features and novel therapies. *Prog Retin Eye Res*. 2021;82:100898.
5. George ND, Yates JR, Moore AT. Clinical features in affected males with X-linked retinoschisis. *Arch Ophthalmol*. 1996;114(3):274–280.
6. Vincent A, Robson AG, Neveu MM, et al. A phenotype-genotype correlation study of X-linked retinoschisis. *Ophthalmology*. 2013;120(7):1454–1464.
7. Andreoli MT, Lim JI. Optical coherence tomography retinal thickness and volume measurements in X-linked retinoschisis. *Am J Ophthalmol*. 2014;158(3):567–573.e2.
8. Georgiou M, Fujinami K, Michaelides M, et al. Retinal imaging in inherited retinal diseases. *Ann Eye Sci*. 2020;5(25). https://doi.org/10.21037/aes-20-81.
9. Gregori NZ, Lam BL, Gregori G, et al. Wide-field spectral-domain optical coherence tomography in patients and carriers of X-linked retinoschisis. *Ophthalmology*. 2013;120(1):169–174.
10. Orès R, Mohand-Said S, Dhaenens CM, et al. Phenotypic characteristics of a French cohort of patients with X-linked retinoschisis. *Ophthalmology*. 2018;125(10):1587–1596.
11. Chen J, Xu K, Zhang X, et al. Novel mutations of the RS1 gene in a cohort of Chinese families with X-linked retinoschisis. *Mol Vis*. 2014;20:132–139.
12. Gao FJ, Dong JH, Wang DD, et al. Comprehensive analysis of genetic and clinical characteristics of 30 patients with X-linked juvenile retinoschisis in China. *Acta Ophthalmol*. 2021;99(4):e470–e479.
13. Bowles K, Cukras C, Turriff A, et al. X-linked retinoschisis: RS1 mutation severity and age affect the ERG phenotype in a cohort of 68 affected male subjects. *Invest Ophthalmol Vis Sci*. 2011;52(12):9250–9256.
14. Menke MN, Feke GT, Hirose T. Effect of aging on macular features of X-linked retinoschisis assessed with optical coherence tomography. *Retina*. 2011;31(6):1186–1192.
15. Lesch B, Szabó V, Kánya M, et al. Clinical and genetic findings in Hungarian patients with X-linked juvenile retinoschisis. *Mol Vis*. 2008;14:2321–2332.
16. Apushkin MA, Fishman GA, Rajagopalan AS. Fundus findings and longitudinal study of visual acuity loss in patients with X-linked retinoschisis. *Retina*. 2005;25(5):612–618.
17. Chen C, Xie Y, Sun T, et al. Clinical findings and RS1 genotype in 90 Chinese families with X-linked retinoschisis. *Mol Vis*. 2020;26:291–298.
18. Eksandh L, Andréasson S, Abrahamson M. Juvenile X-linked retinoschisis with normal scotopic b-wave in the electroretinogram at an early stage of the disease. *Ophthalmic Genet*. 2005;26(3):111–117.
19. Pimenides D, George ND, Yates JR, et al. X-linked retinoschisis: clinical phenotype and RS1 genotype in 86 UK patients. *J Med Genet*. 2005;42(6):e35.
20. Simonelli F, Cennamo G, Ziviello C, et al. Clinical features of X linked juvenile retinoschisis associated with new mutations in the XLRS1 gene in Italian families. *Br J Ophthalmol*. 2003;87(9):1130–1134.
21. Fahim AT, Ali N, Blachley T, Michaelides M. Peripheral fundus findings in X-linked retinoschisis. *Br J Ophthalmol*. 2017;101(11):1555–1559.
22. Genead MA, Fishman GA, Walia S. Efficacy of sustained topical dorzolamide therapy for cystic macular lesions in patients with X-linked retinoschisis. *Arch Ophthalmol*. 2010;128(2):190–197.
23. Kellner U, Brümmer S, Foerster MH, Wessing A. X-linked congenital retinoschisis. *Graefes Arch Clin Exp Ophthalmol*. 1990;228(5):432–437.
24. Roesch MT, Ewing CC, Gibson AE, Weber BH. The natural history of X-linked retinoschisis. *Can J Ophthalmol*. 1998;33(3):149–158.
25. Yang HS, Lee JB, Yoon YH, Lee JY. Correlation between spectral-domain OCT findings and visual acuity in X-linked retinoschisis. *Invest Ophthalmol Vis Sci*. 2014;55(5):3029–3036.
26. Pennesi ME, Birch DG, Jayasundera KT, et al. Prospective evaluation of patients with X-linked retinoschisis during 18 months. *Invest Ophthalmol Vis Sci*. 2018;59(15):5941–5956.
27. Cukras CA, Huryn LA, Jeffrey BG, et al. Analysis of anatomic and functional measures in X-linked retinoschisis. *Invest Ophthalmol Vis Sci*. 2018;59(7):2841–2847.
28. Eriksson U, Larsson E, Holmström G. Optical coherence tomography in the diagnosis of juvenile X-linked retinoschisis. *Acta Ophthalmol Scand*. 2004;82(2):218–223.
29. Gregori NZ, Berrocal AM, Gregori G, et al. Macular spectral-domain optical coherence tomography in patients with X linked retinoschisis. *Br J Ophthalmol*. 2009;93(3):373–378.
30. Ling KP, Mangalesh S, Tran-Viet D, et al. Handheld spectral domain optical coherence tomography findings of X-linked retinoschisis in early childhood. *Retina*. 2020;40(10):1996–2003.
31. Hahn LC, van Schooneveld MJ, Wesseling NL, et al. X-linked retinoschisis: novel clinical observations and genetic spectrum in 340 patients, 00740-5 *Ophthalmology*. 2022;(129):191–202.
32. Daich Varela M, Esener B, Hashem SA, et al. Structural evaluation in inherited retinal diseases. *Br J Ophthalmol*. 2021;105(12):1623–1631.
33. Georgiou M, Kane T, Tanna P, et al. Prospective cohort study of childhood-onset Stargardt disease: fundus autofluorescence imaging, progression, comparison with adult-onset disease, and disease symmetry. *Am J Ophthalmol*. 2020;211:159–175.
34. Georgiou M, Kalitzeos A, Patterson EJ, et al. Adaptive optics imaging of inherited retinal diseases. *Br J Ophthalmol*. 2018;102(8):1028–1035.
35. Georgiou M, Fujinami K, Michaelides M. Inherited retinal diseases: therapeutics, clinical trials and end points—a review. *Clin Exp Ophthalmol*. 2021;49(3):270–288.
36. Ou J, Vijayasarathy C, Ziccardi L, et al. Synaptic pathology and therapeutic repair in adult retinoschisis mouse by AAV-RS1 transfer. *J Clin Invest*. 2015;125(7):2891–2903.

37. Byrne LC, Oztürk BE, Lee T, et al. Retinoschisin gene therapy in photoreceptors, Müller glia or all retinal cells in the Rs1h-/- mouse. *Gene Ther*. 2014;21(6):585–592.

38. Cukras C, Wiley HE, Jeffrey BG, et al. Retinal AAV8-RS1 gene therapy for X-linked retinoschisis: initial findings from a phase I/IIa trial by intravitreal delivery. *Mol Ther*. 2018;26(9):2282–2294.

Pictures & Perspectives

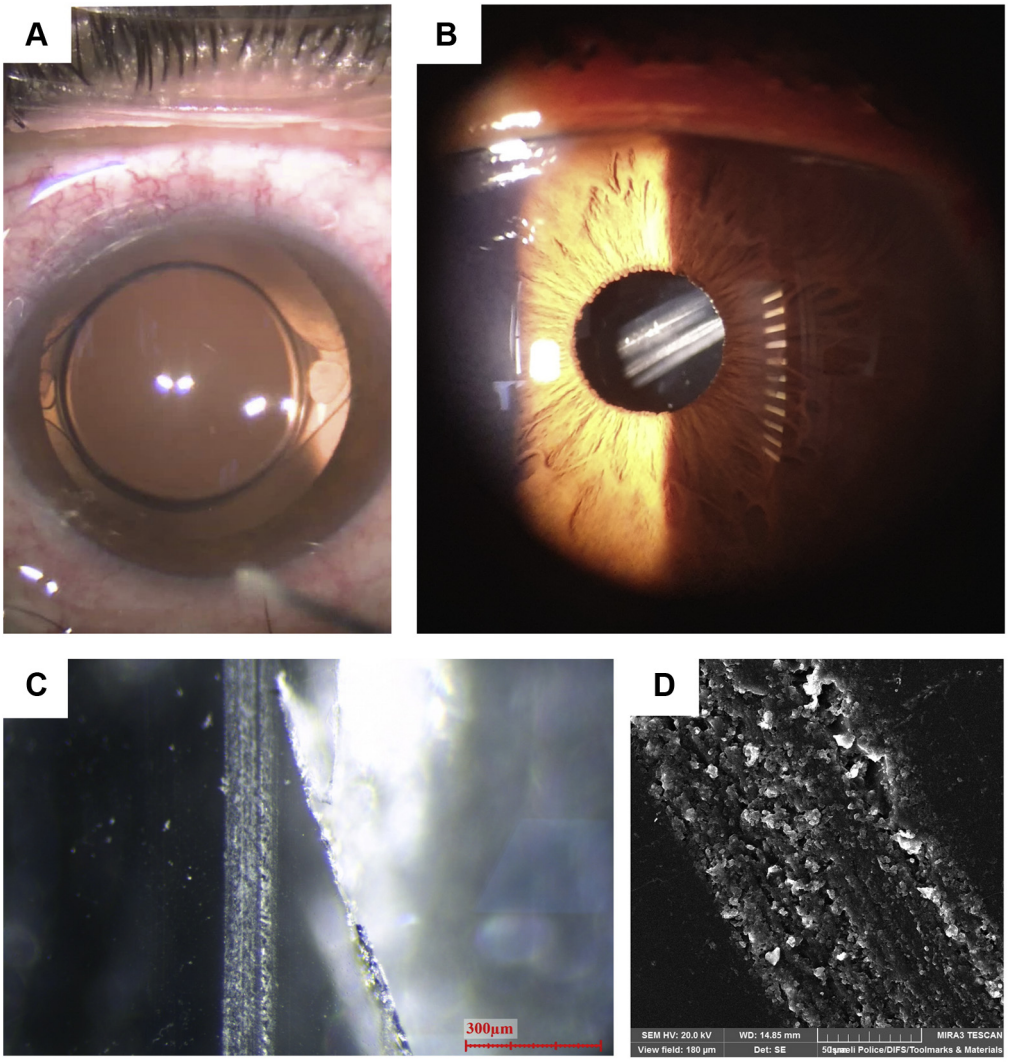

Opacification in a Preloaded Intraocular Lens

A 64-year-old woman underwent uneventful cataract surgery with implantation of enVista IOL (Bausch + Lomb) preloaded single-piece hydrophobic acrylic intraocular lens (IOL) MX60PL (Fig **A**). At 1-day postoperatively, a central diagonal opacity of unknown origin was observed (Fig **B**). After replacement of the lens, significant marks were observed on the lens under standard microscopy (Fig **C**). After IOL-exchange surgery, the visual acuity improved from 20/30 to 20/20. The original lens was sent to a forensic laboratory for evaluation. Electron microscope examination revealed that the opacity was due to abrasions on the surface of the lens (Fig **D**). The X-ray detector found traces of aluminum, which most likely originated in the device that caused the abrasions during loading/injection (Magnified version of Fig **A**-**D** is available online at www.aaojournal.org).

Ari Leshno, MD[1,2,3]
Emmanuel Schwalb, MD[1,2]

[1]Goldschleger Eye Institute, Sheba Medical Center, Tel-Hashomer, Israel; [2]The Sackler Faculty of Medicine, Tel Aviv University, Tel Aviv, Israel; [3]The Sheba Talpiot Medical Leadership Program, Tel Hashomer, Israel